Article

Cell Metabolism

Mitochondria Restrict Growth of the Intracellular Parasite *Toxoplasma gondii* by Limiting Its Uptake of Fatty Acids

Graphical Abstract

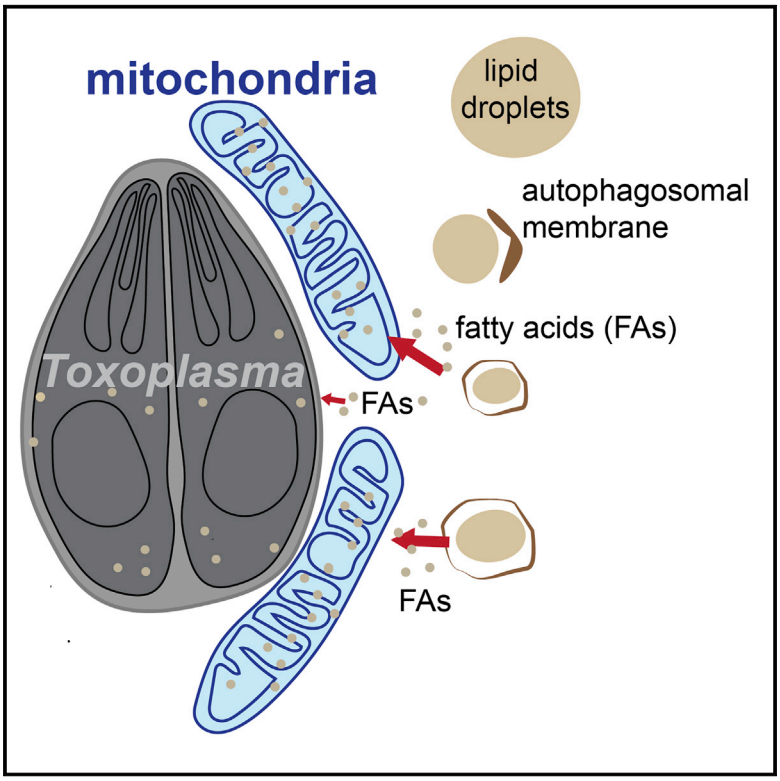

Authors

Lena Pernas, Camilla Bean, John C. Boothroyd, Luca Scorrano

Correspondence

luca.scorrano@unipd.it

In Brief

Intracellular microbes harness essential metabolites from the host cell. In this issue, Pernas et al. show that mitochondria mount a metabolic defense against the intracellular parasite *Toxoplasma gondii* by fusing around its vacuole and siphoning fatty acids that *Toxoplasma* liberates by activating autophagy of host lipid droplets.

Highlights

- Toxoplasma exploits host lipophagy to acquire fatty acids (FAs)
- Host lipid metabolism modulates parasite growth
- Host mitochondria compete with *Toxoplasma*, taking up FAs early during infection
- Mitochondrial fusion limits parasite growth by restricting parasite access to FAs

Pernas et al., 2018, Cell Metabolism *27*, 886–897
April 3, 2018
https://doi.org/10.1016/j.cmet.2018.02.018

CellPress

CellPress

Cell Metabolism
Article

Mitochondria Restrict Growth of the Intracellular Parasite *Toxoplasma gondii* by Limiting Its Uptake of Fatty Acids

Lena Pernas,[1,2] Camilla Bean,[1,2] John C. Boothroyd,[3] and Luca Scorrano[1,2,4,*]
[1]Department of Biology, University of Padova, 35121 Padova, Italy
[2]Venetian Institute of Molecular Medicine, 35129 Padova, Italy
[3]Department of Microbiology and Immunology, Stanford University, Stanford, CA 94305, USA
[4]Lead Contact
*Correspondence: luca.scorrano@unipd.it
https://doi.org/10.1016/j.cmet.2018.02.018

SUMMARY

How intracellular pathogens acquire essential non-diffusible host metabolites and whether the host cell counteracts the siphoning of these nutrients by its invaders are open questions. Here we show that host mitochondria fuse during infection by the intracellular parasite *Toxoplasma gondii* to limit its uptake of fatty acids (FAs). A combination of genetics and imaging of FA trafficking indicates that *Toxoplasma* infection triggers lipophagy, the autophagy of host lipid droplets (LDs), to secure cellular FAs essential for its proliferation. Indeed, *Toxoplasma* FA siphoning and growth are reduced in host cells genetically deficient for autophagy or triglyceride depots. Conversely, *Toxoplasma* FA uptake and proliferation are increased in host cells lacking mitochondrial fusion, required for efficient mitochondrial FA oxidation, or where mitochondrial FA oxidation is pharmacologically inhibited. Thus, mitochondrial fusion can be regarded as a cellular defense mechanism against intracellular parasites, by limiting *Toxoplasma* access to host nutrients liberated by lipophagy.

INTRODUCTION

Obligate intracellular pathogens depend on host cell-derived nutrients for survival. Limiting their ability to acquire specific nutrients can inhibit their growth or induce a dormant state (Abu Kwaik and Bumann, 2015; Fox et al., 2004). Unlike for small-molecule metabolites that can freely diffuse in the host cell cytoplasm, the uptake of host fatty acids (FAs) poses a unique challenge to intracellular microbes for two key reasons: (1) FAs are largely sequestered as triglycerides in membrane-bound lipid droplets (LDs), and (2) mitochondria, the metabolic hubs of eukaryotic cells where β-oxidation takes place, are a major destination for FAs from LDs (Herms et al., 2015; Rambold et al., 2015; Walther and Farese, 2012). How a microbe gains access to membrane-bound host FAs, and whether host organelles such as mitochondria can counter nutrient siphoning, are unanswered questions applicable to the study of most host-pathogen interactions.

Mitochondrial functional versatility is largely mediated by changes in morphology. For example, cytosolic signals can regulate the efficiency of fuel usage by mitochondria by impinging on fission, fusion, and cristae remodeling (Pernas and Scorrano, 2016). During starvation, when autophagy is induced to liberate nutrients and mobilize FAs from LDs that undergo lipophagy, mitochondria elongate and their cristae surface increases, to evade autophagic degradation and maximize efficiency of ATP production (Gomes et al., 2011; Rambold et al., 2011; Reggiori and Klionsky, 2002; Singh et al., 2009; Patten et al., 2014). Furthermore, these morphological changes enhance the efficiency of β-oxidation by increasing mitochondrial association with and uptake of FAs from LDs (Herms et al., 2015; Rambold et al., 2015).

Intriguingly, host mitochondria traffic to the vacuoles, where several intracellular evolutionarily divergent prokaryotic and eukaryotic pathogens, including the bacteria *Legionella pneumophila* and *Chlamydia psitacci*, and the parasite *Toxoplasma gondii* (Brieland et al., 1997; Friis, 1972; Hacker et al., 2014; Horwitz, 1983; Jones and Hirsch, 1972), grow and divide (Dumoux and Hayward, 2016). *Toxoplasma* infects one-third of humans and an unparalleled range of animals (Montoya and Liesenfeld, 2004). Like *Chlamydia*, it prolifically scavenges host lipid species (Caffaro and Boothroyd, 2011; Charron and Sibley, 2002; Coccchiaro et al., 2008; Coppens et al., 2000; Ramakrishnan et al., 2012; Romano et al., 2013). Morphology of mitochondria in response to infection depends on the microbe studied: mitochondria elongate around the *Toxoplasma* vacuole (Pernas et al., 2014); in contrast, they fragment following *Listeria* entry (Stavru et al., 2011) or *Vibrio cholerae* infection (Suzuki et al., 2014), a process essential to promote their growth. Why mitochondria elongate early around the *Toxoplasma* vacuole is not understood.

Using *Toxoplasma* to study the relationship among an intracellular microbe, access to essential lipids, and mitochondrial morphology, we show that *Toxoplasma* co-opts host cell lipophagy to obtain FAs needed for its proliferation. Host mitochondria conversely fuse around the parasite vacuole, siphoning FA from *Toxoplasma* and restricting its growth. Our results identify mitochondrial fusion and FA metabolism as an important defense against an intracellular parasite.

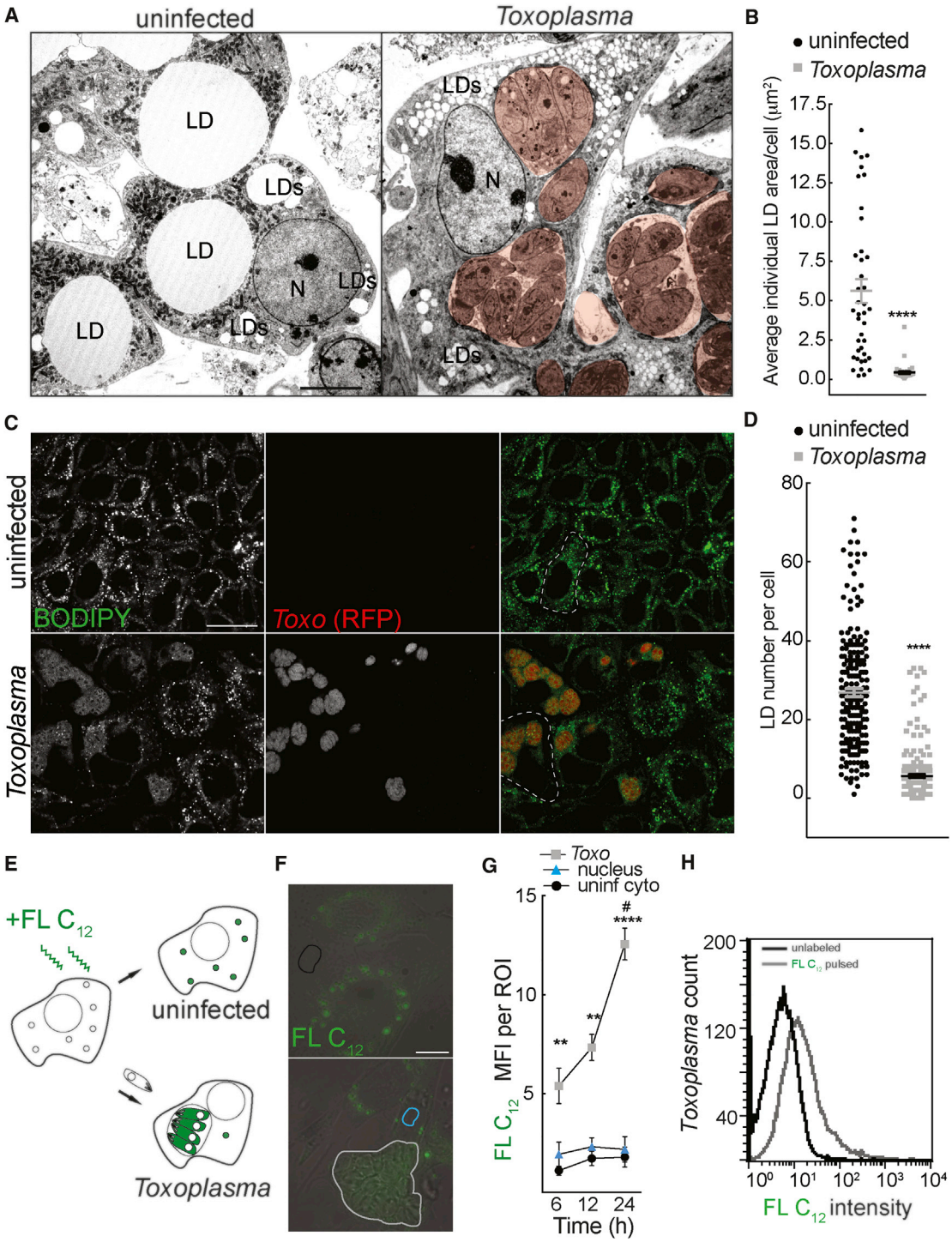

Figure 1. *Toxoplasma* Depletes Host LDs and Accumulates LD-Derived FAs

(A) Electron micrographs of mouse primary adipocytes 24 hr post-mock or *Toxoplasma* infection. *Toxoplasma* vacuoles are pseudocolored red. Scale bar, 5 μm.

(B) Dot plot of the average area of an individual lipid droplet (LD) in n = 40 cells in experiments as in (A). Means ± SEM are plotted. ****$p < 0.0001$ in an unpaired t test.

(C) Confocal images of mock- and *Toxoplasma* RFP$^+$ (red)-infected Caco-2 cells labeled with BODIPY493/503 (green) and imaged 24 hr post-infection (hpi). Selected cells are contoured by a dashed line in merged panels. Scale bar, 25 μm.

(D) Dot plot of LD number in experiments as in (C) in n = 200 cells. Means ± SEM are plotted. ****$p < 0.0001$ in an unpaired t test.

(E) Schematic representation of fluorescent FA-pulse and infection-chase assay. MEFs were incubated overnight with FL C_{12}, rinsed, mock- or *Toxoplasma*-infected, and analyzed by flow cytometry or fluorescence microscopy.

(legend continued on next page)

RESULTS

Toxoplasma Depletes Host LDs and Accumulates LD-Derived FAs

Toxoplasma proliferates within a membrane-bound vacuole and scavenges host FAs (Caffaro and Boothroyd, 2011; Charron and Sibley, 2002). Because FAs are largely stored in LDs as triglycerides and LDs traffic to the vacuoles where *Toxoplasma* and several intracellular pathogens grow (Cocchiaro et al., 2008; Mota et al., 2014; Nolan et al., 2017; Rabhi et al., 2016), we speculated that *Toxoplasma* acquires FAs from host LDs. LDs are dynamically remodeled when FAs are required for energy conversion or biosynthesis of complex molecules (Walther and Farese, 2012). To determine the fate of host LDs during *Toxoplasma* infection, we turned to adipocytes that contain large LDs whose dynamics are clear. Electron microscopy (EM) analysis revealed that LDs with a surface >5 μm^2 were almost completely lost in adipocytes harboring *Toxoplasma* vacuoles (Figures 1A and 1B). We extended these findings by confocal imaging of LDs labeled with the neutral lipid marker BODIPY 493/503 in *Toxoplasma*-infected human intestinal epithelium Caco-2 cells (Figures 1C and 1D), murine embryonic fibroblasts (MEFs) (Figures S1A and S1B), and myoblasts (data not shown). Thus, *Toxoplasma* infection of mammalian cells results in LD shrinkage.

We next ascertained whether the observed loss of host LDs was a consequence of trafficking of host LD-derived FAs to *Toxoplasma*. Cells pulsed with BODIPY-FL-C_{12} (FL C_{12}), a 12-carbon saturated FA covalently bound to the BODIPY fluorophore at its hydrophobic end (hence equivalent to a long-chain FA), esterify it in LDs, enabling subsequent tracking of LD-derived FAs (Figure 1E) (Rambold et al., 2015). During infection, FL C_{12} was significantly and increasingly rerouted to the vacuole of live *Toxoplasma* as dead parasites did not take up the fluorescent FA (Figures 1F, 1G, and S1C). Of note, we did not observe an increase in FL C_{12} fluorescence in the cytosol of uninfected cells or in the nuclei of infected cells, supporting that host FAs liberated from host LDs specifically accumulate in the parasite vacuole. Furthermore, flow cytometry confirmed that parasites isolated from MEFs pulsed with FL C_{12} before infection accumulated the fluorescent FA FL C_{12} (Figure 1H). Together, these data show that during infection host FAs are depleted from LDs and taken up by *Toxoplasma*.

Lipophagy in Host Cells Infected with *Toxoplasma*

Intact host LDs have been visualized in *Chlamydia* and *Leishmania* vacuoles during infection (Cocchiaro et al., 2008; Rabhi et al., 2016), and *Toxoplasma* internalizes host LDs into the parasite vacuole following supplementation of infected cells with exogenous FAs (Nolan et al., 2017). However, host LDs that were labeled with FL C_{12} were not evident in the *Toxoplasma* vacuole at early, middle, or late stages of infection (Figure 1F), suggesting that LD catabolism preceded host FA acquisition by *Toxoplasma*. LDs can be degraded by autophagy to provide FAs to fuel mitochondrial β-oxidation (Farese and Walther, 2009; Herms et al., 2015; Rambold et al., 2015; Singh et al., 2009). Because host autophagy is induced during *Toxoplasma* infection and contributes to parasite proliferation (Gao et al., 2014; Souto et al., 2016; Wang et al., 2009), we posited that *Toxoplasma* exploits lipophagy, i.e., the autophagy of LDs, to acquire host FAs from LDs. We first confirmed that *Toxoplasma* induces autophagy in MEFs (Figures S2A and S2C), human foreskin fibroblasts (Figure S2B), and Caco-2 (Figure S2D), whose LD population is depleted at late stages of *Toxoplasma* infection (Figures 1C and 1D). We then asked whether *Toxoplasma* triggered lipophagy by testing whether LDs associate with autophagosomes during infection. Levels of Perilipin-3-RFP^+ LD apposition to LC3-GFP^+ autophagosomes were increased 2- to 3-fold (Figures 2A and 2B) at early and middle stages of infection. As expected, these structures were lost later during infection (Figures 2A and 2B), when LDs disappear (Figures 1C, 1D, S1A, and S1B). Finally, EM analysis of *Toxoplasma*-infected MEFs retrieved circular electron-transparent structures identifiable as LDs in autophagosomes (Figures 2C and 2D). Thus, lipophagy occurs during *Toxoplasma* infection.

Lipophagy Promotes *Toxoplasma* Acquisition of FAs

We next wished to evaluate the role of host lipophagy in *Toxoplasma* FA acquisition. As lipophagy receptors have not yet been identified, we addressed whether the loss of host cell autophagy affected *Toxoplasma* uptake of host FAs. Imaging and flow cytometry revealed that parasites isolated from *Atg7*$^{-/-}$ MEFs that are deficient in macroautophagy (Komatsu et al., 2005) accumulated ~50% less RC_{12} (another 12-carbon chain saturated FA) and FL C_{12} than parasites from *Atg7*$^{+/+}$ MEFs (Figures 3A–3D). To confirm the importance of LDs as a source for lipids for *Toxoplasma*, we examined the acquisition of FAs by parasites in diglyceride acyltransferases 1 and 2 knockout MEFs (*Dgat1*$^{-/-}$,*2*$^{-/-}$), which are deficient in lipid storage due to impaired triglyceride synthesis and LD formation (Harris et al., 2011). We found that parasites took up significantly less FL C_{12} in *Dgat1*$^{-/-}$,*2*$^{-/-}$ MEFs (Figures 3E and 3F). Conversely, the inhibition of the cytoplasmic adipose triglyceride lipase (ATGL) with atglistatin (Mayer et al., 2013) did not decrease FA uptake by *Toxoplasma* (Figure S3), indicating that ATGL-mediated lipolysis is not required for parasitic acquisition of FAs. These data support that *Toxoplasma* exploits host lipophagy to acquire FAs.

Loss of Host Cell Autophagy and Triglyceride Storage Limits *Toxoplasma* Growth

Toxoplasma metabolizes and incorporates host FAs into storage organelles and dividing membranes, two important processes for parasite proliferation (Caffaro and Boothroyd, 2011; Charron

(F) Combined bright-field epifluorescence images of FL C_{12}-pulsed cells at 24 hpi. Representative regions of interest (ROIs) used to quantify the mean fluorescence intensity (MFI) are outlined in black (uninfected cells cytoplasm), blue (infected cells nuclei), or gray (*Toxoplasma* vacuoles). Scale bar, 10 μm.
(G) Mean ± SEM from n = 3 independent experiments of relative FL C_{12} accumulation in ROIs of uninfected cells cytosol or *Toxoplasma* vacuoles in experiments as in (F). $^{**}p < 0.01$, $^{****}p < 0.0001$ *Toxoplasma* vacuole versus uninfected cytosol, $^{\#}p < 0.001$ 6 hpi versus 24 hpi by two-way ANOVA.
(H) Histograms of FL C_{12} MFI determined by flow cytometry of *Toxoplasma*:RFP^+ isolated at 24 hpi from unpulsed (black line) and FL C_{12}-pulsed MEFs (gray line).
See also Figure S1.

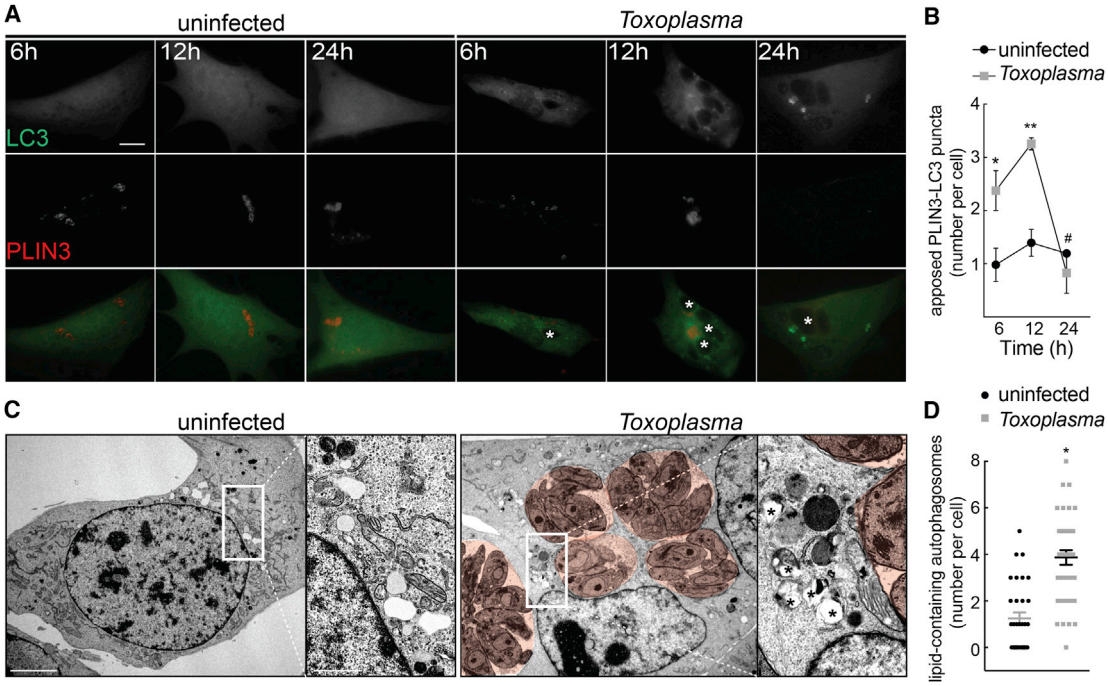

Figure 2. *Toxoplasma* Infection Triggers Lipophagy

(A) Representative fluorescent images of MEFs expressing LC3-GFP (green) and PLIN3-RFP (red) fixed and imaged at the indicated time points following infection. *Toxoplasma* vacuoles (identified from bright-field images) are labeled with white asterisks in the merged images. Scale bar, 10 μm.

(B) Dot plot of the number of apposed LC3-PLIN3 puncta per cell in experiments as in (A). Mean ± SEM is plotted. *$p < 0.05$, **$p < 0.01$ infected versus uninfected, #$p < 0.05$ 24 hpi versus 6 hpi by two-way ANOVA.

(C) EMs of uninfected and *Toxoplasma*-infected wild-type MEFs at 24 hpi. *Toxoplasma* vacuoles are pseudocolored red; lipid-containing autophagosomes are marked with asterisks. Scale bars, 5 μm (main panel) and 2 μm (inset).

(D) Dot plot of the number of lipid-containing autophagosomes determined from n = 40 EMs acquired as in (C). Mean ± SEM is indicated. *$p < 0.05$ in an unpaired t test.

See also Figure S2.

and Sibley, 2002; Ramakrishnan et al., 2015). We reasoned that decreased FA acquisition might negatively affect *Toxoplasma* growth in *Atg7*$^{-/-}$ MEFs, irrespective of the beneficial effect of autophagy against certain intracellular pathogens (Deretic, 2011), including *Toxoplasma* (Andrade et al., 2006; Late et al., 2017).

To evaluate parasite growth, we devised a flow cytometry-based approach using *Toxoplasma*-derived RFP as a readout for parasite burden. Following infection with *RFP*$^{+}$-*Toxoplasma* at a low MOI of 2, monolayers were rinsed 2 hr post-infection (hpi) and analyzed at 24 hpi, a time after several replication cycles but before the initiation of cellular lysis and, thus, of reinvasion events (Black and Boothroyd, 2000). We verified that under these conditions the RFP readout reflected parasite proliferation within one growth cycle, rather than multiply infected cells, asynchronous infection, or reinfection of neighboring cells. A significant reduction in *Toxoplasma* burden was observed by microscopy and flow cytometry at 24 hpi, but not prior to replication events in cells treated with the parasite growth inhibitor pyrimethamine (Derouin and Chastang, 1989), demonstrating that RFP fluorescence is a reliable readout of *Toxoplasma* proliferation (Figure S4). Using this approach, we found that at 24 hpi the *Toxoplasma* burden in *Atg7*$^{-/-}$ MEFs was ~30% lower than in *Atg7*$^{+/+}$ MEFs. Supplementation at 2 hpi of BSA-conjugated unsaturated FAs oleate and linoleate (Figure 4C), for which *Toxoplasma* is predicted to be auxotrophic (Tymoshenko et al., 2015), partially reverted the parasite growth defect in *Atg7*$^{-/-}$ MEFs (Figures 4A and 4B). Thus, autophagy enables the acquisition of LD-derived FAs important for the growth of *Toxoplasma*.

Toxoplasma proliferation was also reduced in LD-deficient *Dgat1*$^{-/-}$,*2*$^{-/-}$ MEFs (Figures 4D and 4E). The addition of exogenous FAs plus cholesterol, whose levels are reduced in *Dgat1*$^{-/-}$,*2*$^{-/-}$ MEFs (Harris et al., 2011) and whose esterification is important for *Toxoplasma* growth (Sonda et al., 2001), abolished the *Toxoplasma* growth defect in these MEFs (Figure 4F). The slower *Toxoplasma* growth in *Atg7*$^{-/-}$ or *Dgat1*$^{-/-}$,*2*$^{-/-}$ MEFs was not caused by differences in invasion because the burden of parasites prior to replication events (2 hpi) was unaffected in both cell lines (Figure S5). These results support a model whereby host lipophagy supplies FAs and cholesteryl esters for *Toxoplasma* growth.

Toxoplasma Growth Depends on Host Cell Lipid Storage

To further corroborate the role of host LD-derived FAs in *Toxoplasma* growth, we manipulated host lipid metabolism. We reasoned that diverting host FAs toward their accumulation in LDs might phenocopy the slower growth of *Toxoplasma* observed in *Dgat1*$^{-/-}$,*2*$^{-/-}$ MEFs deficient for FA storage.

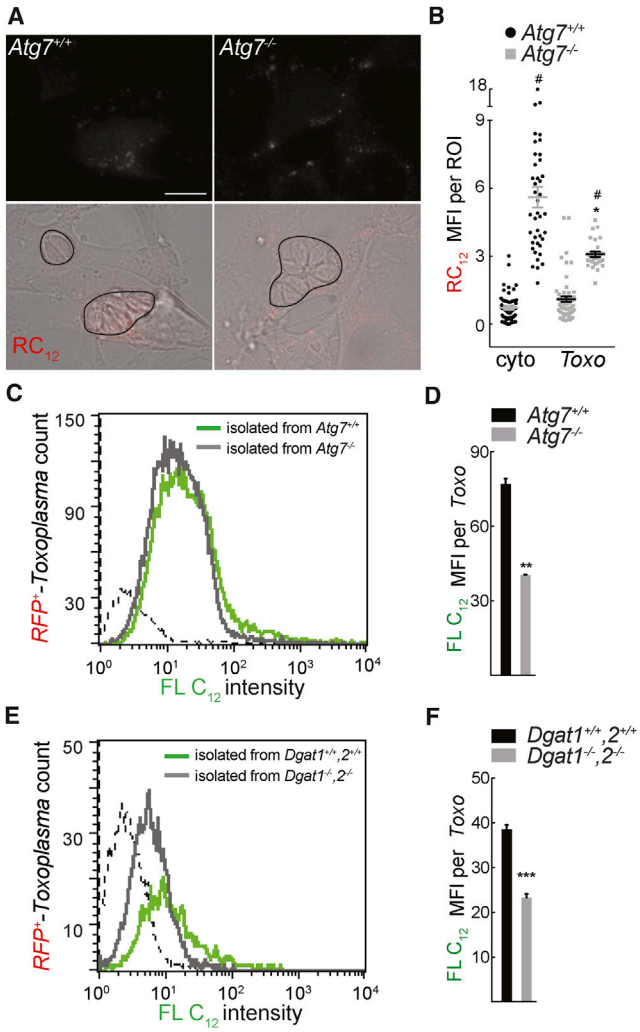

Figure 3. *Toxoplasma* Acquires FAs by Promoting Host Lipophagy

(A) RC_{12} and merged bright-field and fluorescence images of MEFs of the indicated genotype. Cells were pulsed with RC_{12} and mock- or *Toxoplasma*-infected, fixed, and imaged at 24 hpi. *Toxoplasma* vacuoles are outlined in black. Scale bar, 10 μm.

(B) RC_{12} accumulation in cytosol (cyto) of uninfected MEFs of the indicated genotype or in *Toxoplasma* vacuoles (Toxo) of infected cells at 24 hpi. Data are mean + SEM of n = 3 experiments as in (A). $^{\#}p < 0.05$ for *Toxoplasma* vacuole versus uninfected cytoplasm, $^{*}p < 0.05$ for $Atg7^{+/+}$ versus $Atg7^{-/-}$ by two-way ANOVA.

(C and D) Flow histogram (C) and flow cytometry analysis (D) of FLC_{12} MFI in RFP^{+}-*Toxoplasma* isolated from FLC_{12}-pulsed MEFs of the indicated genotype at 24 hpi. Dotted line in (C) is the background fluorescence of parasites isolated from unlabeled MEFs. Data are mean + SEM from n = 3 independent experiments, $^{**}p < 0.01$ by unpaired t test.

(E and F) Flow histogram (E) and flow cytometry analysis (F) of FL C_{12} MFI in RFP^{+}-*Toxoplasma* isolated from FL C_{12}-pulsed $Dgat1^{+/+},2^{+/+}$ and $Dgat1^{-/-},2^{-/-}$ MEFs at 24 hpi. Dotted line in (E) is the background fluorescence of parasites isolated from unlabeled MEFs. Data are mean + SEM from n = 3 independent experiments, $^{***}p < 0.001$ by unpaired t test.

See also Figure S3.

Because addition of free, long-chain unsaturated FAs to cells increases triglyceride levels and LD accumulation (Fujimoto et al., 2006; Rohwedder et al., 2014), we infected MEF monolayers and supplemented them with free linoleic acid (LA) at 2 hpi, when parasites were intracellular, to avoid possible toxic effects on non-internalized parasites. LA triggered the expected LD formation (Figure 5A) and, strikingly, halved parasite growth (Figure 5B). If the LA treatment reduced *Toxoplasma* growth by driving FA sequestration and esterification into LDs, the induction of lipophagy would reverse it. Indeed, when we stimulated lipophagy by removing lipids from culture media (Rambold et al., 2015; Singh et al., 2009), the LD formation and *Toxoplasma* growth defect induced by LA treatment were reversed (Figures 5A and 5B), and FA uptake by the parasites was promoted (Figures 5C and 5D). Finally, the removal of lipids following infection increased parasite burden in $Atg7^{+/+}$, but not $Atg7^{-/-}$, MEFs, further supporting the role of lipophagy in supplying *Toxoplasma* with lipids important for its growth (Figure S6A).

Early Host Mitochondrial FA Uptake Restricts *Toxoplasma* Proliferation

Manipulations of FA metabolism, e.g., by inducing lipid storage or catabolism, have been posited as an approach to diminish FA availability in cancer cells (Currie et al., 2013). We extrapolated this framework to *Toxoplasma* infection and reasoned that if our model was correct, modulation of FA availability might affect parasite growth. Indeed, the peroxisome proliferator-activated receptor δ agonist GW0742, which promotes FA catabolism (Sznaidman et al., 2003), or insulin, which promotes FA storage, decreased *Toxoplasma* burden (Figure 5E). In contrast, a block in acyl-coenzyme A (CoA) entry into mitochondria via etomoxir inhibition of carnitine-palmitoyl CoA transferase I (CPT1) (Lopaschuk et al., 1988) stimulated *Toxoplasma* growth (Figure 5F). We tested the possibility that fatty acid oxidation (FAO) inhibition created a permissive environment for parasite replication by reducing mitochondrial reactive oxygen species (ROS) production. The mitochondrial ROS scavenger MitoTEMPO (Leanza et al., 2017) slightly favored parasite proliferation in untreated cells, but did not affect the etomoxir-induced increase in *Toxoplasma* growth (Figure 5F). We therefore reasoned that the *Toxoplasma* growth-promoting effects of etomoxir were linked to its inhibition of FAO and examined the role of mitochondrial morphology, which regulates mitochondrial FA uptake, in parasite growth.

Mitochondria associate with the vacuole of several prokaryotic and eukaryotic microbes including *Toxoplasma* (Dumoux and Hayward, 2016), around which they elongate (Pernas et al., 2014). At 6 hpi mitochondria appeared elongated and surrounded the parasite vacuole. Interestingly, etomoxir slightly decreased mitochondrial size during *Toxoplasma* infection (Figures 6A–6C). The elongation of mitochondria during *Toxoplasma* infection is reminiscent of that required for mitochondrial FAO during starvation (Gomes et al., 2011; Rambold et al., 2011, 2015). By pulsing cells with RC_{12}, we recorded increased RC_{12} uptake at 6 hpi in mitochondria around *Toxoplasma* vacuoles, compared with mitochondria in uninfected cells (Figures 6A, 6B, and 6D). Treatment with etomoxir (Figures 6A, 6B, and 6D) or an inhibitor of autophagy (Figures S6C–S6E) prevented this observed increase in mitochondrial RC_{12} uptake. Later (24 hpi), mitochondria in *Toxoplasma*-infected cells were fragmented (Syn et al., 2017) and exhibited less overlap with RC_{12} (Figures 7E–7H), likely due to the accumulation of RC_{12} in the parasite vacuoles. Etomoxir

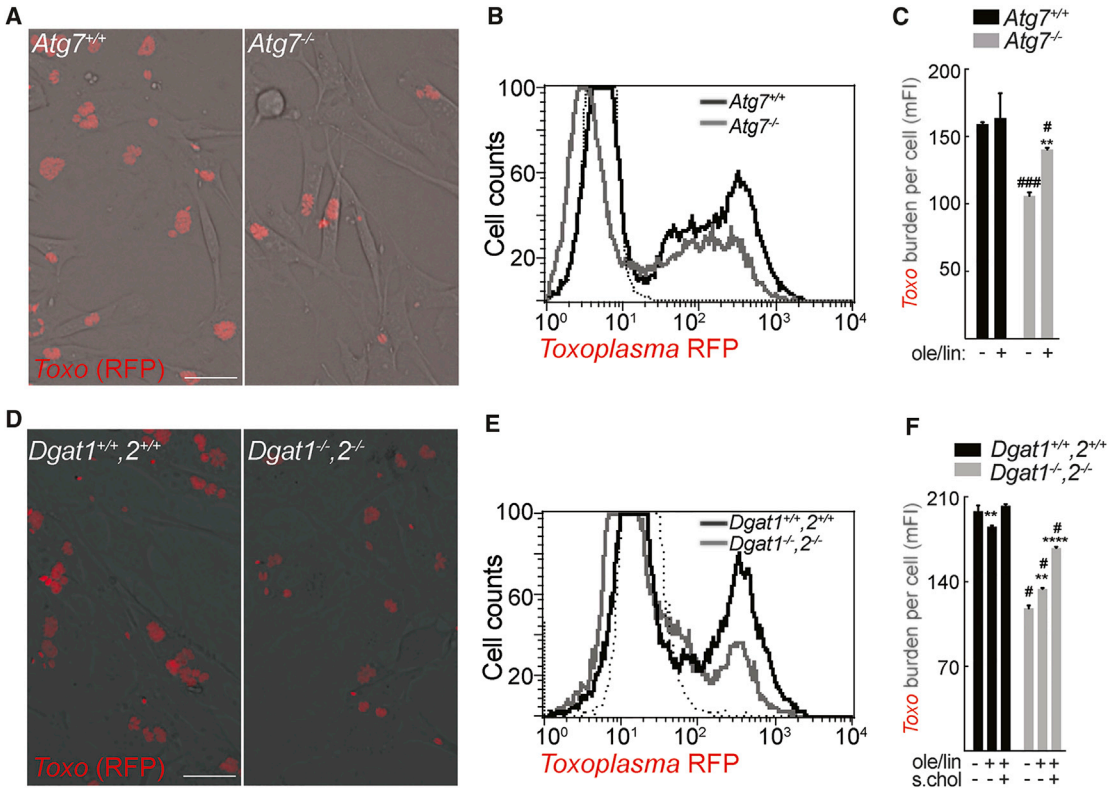

Figure 4. Efficient *Toxoplasma* Growth Requires Host Autophagy and Triglycerides

(A) Representative combined bright-field epifluorescence images of MEFs of the indicated genotype 24 hpi with *RFP*$^{+}$-*Toxoplasma*. Cells were rinsed at 2 hpi and incubated in complete medium without parasites. Scale bar, 25 μm.

(B) Representative flow cytometry histogram of RFP channel at 24 hpi in *RFP*$^{+}$-*Toxoplasma*-infected MEFs of the indicated genotype. Dotted line indicates background fluorescence in uninfected MEFs.

(C) Experiments were as in (B) except that at 2 hpi, MEFs were supplemented with 1 mg/mL fraction V BSA or 30 μM oleate-linoleate-albumin (ole/lin) and analyzed by flow cytometry for median *RFP*$^{+}$-*Toxoplasma* burden (mFI). Data are mean + SEM from n = 3 independent experiments, $^{**}p < 0.01$ treated versus untreated, $^{\#}p < 0.05$, $^{\#\#\#}p < 0.001$, wild-type versus *Atg7*$^{-/-}$ by two-way ANOVA.

(D) Representative combined bright-field epifluorescence images of MEFs of the indicated genotype 24 hpi with *RFP*$^{+}$-*Toxoplasma* (MOI = 2). Cells were rinsed at 2 hpi. Scale bar, 25 μm.

(E) Flow cytometry histogram of RFP channel at 24 hpi in *RFP*$^{+}$-*Toxoplasma*-infected MEFs of the indicated genotype. Dotted line indicates background fluorescence in uninfected MEFs.

(F) Experiments were as in (E) except that at 2 hpi MEFs were supplemented where indicated with 1 mg/mL fraction V BSA, 30 μM oleate acid-linoleate-albumin (ole/lin), or ole/lin and 1× SyntheChol (s.chol), and analyzed at 24 hpi by flow cytometry for *Toxoplasma* burden (RFP mFI). Data are mean + SEM from n = 3 independent experiments, $^{**}p < 0.01$, $^{****}p < 0.0001$ treated versus untreated, $^{\#}p < 0.0001$ *Dgat1*$^{+/+}$,*2*$^{+/+}$ versus *Dgat1*$^{-/-}$,*2*$^{-/-}$ by two-way ANOVA.

See also Figure S4.

treatment, which promoted parasite growth, caused a decrease in the perimeter length and an increase in circularity of mitochondria, hallmarks of mitochondrial fragmentation (Figures 6E–6G). Furthermore, etomoxir increased RC_{12} staining of intra-parasite organelles, supporting that parasites acquire more FAs when their host cells are unable to perform FAO (Figures 6E, 6F, and 6H). These results support a model in which mitochondrial FA metabolism during *Toxoplasma* infection controls parasite growth by limiting its access to liberated host FAs.

Mitochondrial Fusion Restricts *Toxoplasma* Growth and Access to FAs

Mitochondrial fusion is required to distribute and oxidize FAs from LDs during nutrient deprivation. To test the possibility that host mitochondrial remodeling restricted parasite growth by limiting its FA uptake, we first defined the molecular mechanism underlying the observed mitochondrial network morphology changes. Mitochondria in MEFs lacking the outer membrane pro-fusion proteins Mitofusin 1 and 2 (*Mfn1*$^{-/-}$,*2*$^{-/-}$) did not elongate around parasite vacuoles at 6 hpi, as determined by confocal microscopy (Figure 7A), or at 12 hpi as determined by morphometric analysis of EM images (Figures 7B and 7C). At later infection time points, however, mitochondria in *Mfn1*$^{+/+}$,*2*$^{+/+}$ MEFs were fragmented and more similar in length to mitochondria from *Mfn1*$^{-/-}$,*2*$^{-/-}$ MEFs, confirming that mitochondria use their core fusion machinery to elongate around the vacuole early during infection.

We next tested the consequence of mitochondrial fusion manipulation on mitochondrial FA uptake and parasite growth. In *Mfn1*$^{-/-}$,*2*$^{-/-}$ MEFs, mitochondrial FA uptake was undetectable

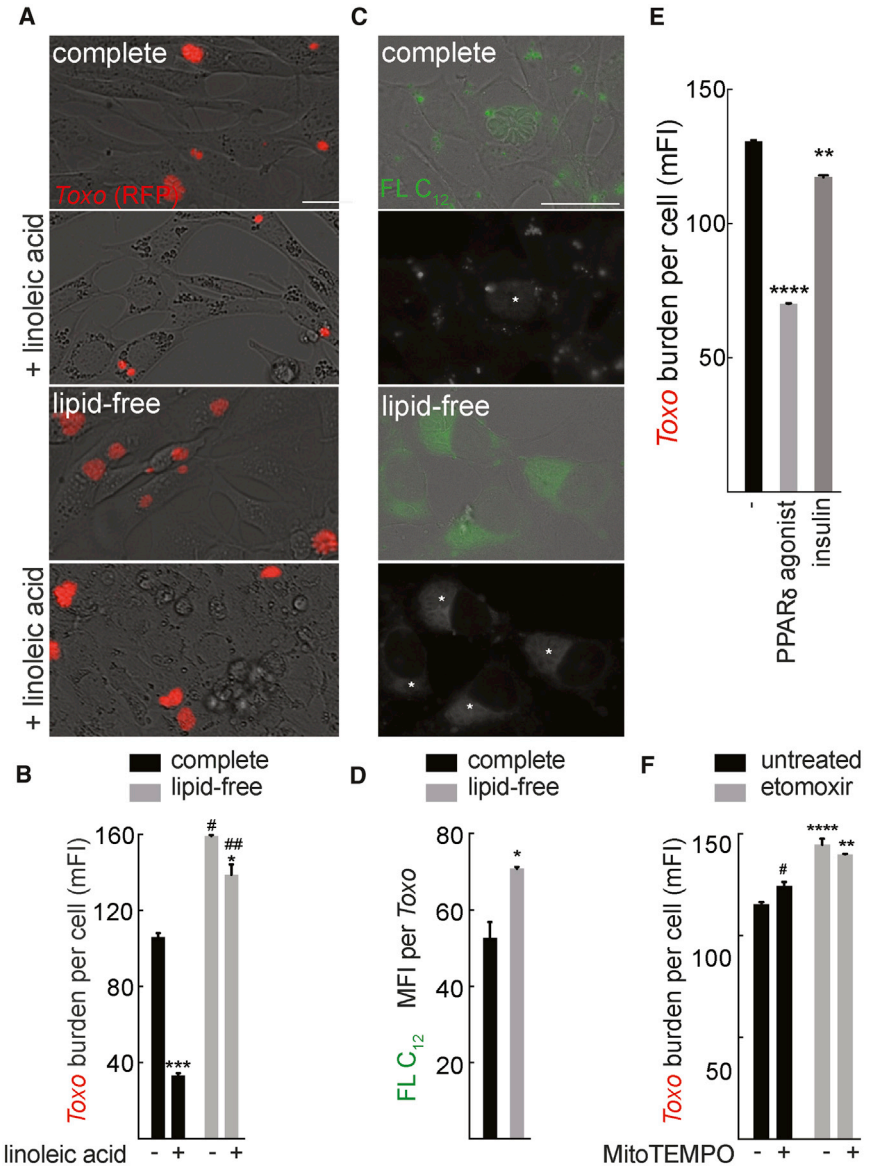

Figure 5. Host Cell Lipid Storage and Mobilization Define *Toxoplasma* Growth

(A) Representative combined bright-field epifluorescence images of wild-type MEFs at 24 hpi with *RFP*$^{+}$-*Toxoplasma* (MOI = 2). MEFs were rinsed at 2 hpi and incubated with medium supplemented where indicated with 0.32 mM free linoleic acid. Scale bar, 25 μm.

(B) Experiments were as in (A) except that MEFs were analyzed by flow cytometry for *Toxoplasma* burden (RFP MFI). Data are mean + SEM of n = 3 experiments, ***p < 0.001 LA-treated versus untreated, $^{\#}$p<0.001, $^{\#\#}$p < 0.0001 lipid-free versus with complete media by two-way ANOVA.

(C) Merged bright-field and fluorescence images of FL C_{12}-pulsed MEFs infected with *Toxoplasma*. Infected monolayers were rinsed at 2 hpi, incubated with the indicated medium, fixed, and imaged at 24 hpi. *Toxoplasma* vacuoles are indicated by asterisks. Scale bar, 20 μm.

(D) FACS analysis of FL C_{12} MFI of *RFP*$^{+}$-*Toxoplasma* isolated from experiments as in (C). Data are mean + SEM of n = 3 experiments, *p < 0.05 by unpaired t test.

(E) MEFs were infected with *RFP*$^{+}$-*Toxoplasma* (MOI = 2), rinsed at 2 hpi, incubated with indicated treatments, and analyzed at 24 hpi by flow cytometry for *Toxoplasma* burden (RFP mFI). Data are mean + SEM of n = 3 experiments, **p < 0.01, ****p < 0.0001 treated versus untreated by one-way ANOVA.

(F) MEFs were infected with *RFP*$^{+}$-*Toxoplasma* (MOI = 2), rinsed at 2 hpi, treated as indicated, and analyzed at 24 hpi by flow cytometry for *Toxoplasma* burden (RFP mFI). Data are mean + SEM of n = 3 experiments, $^{\#}$p < 0.05 MitoTEMPO-treated versus untreated, **p < 0.01, ****p < 0.0001 etomoxir-treated versus untreated, by two-way ANOVA.

See also Figure S5.

at 6 hpi (Figures S7A and S7B), and accordingly, *Toxoplasma* took up more FA (Figure 7D) and grew more efficiently as determined by fluorescence-activated cell sorting (FACS) analysis (Figure 7E), plaque size analysis (Figures S7C and S7D), and parasite per vacuole count (Figure S7E). Because the multiple mitochondrial defects caused by chronic ablation of fusion might confound the interpretation of these results, we confirmed that parasite burden was increased in *Mfn1*$^{flx/flx}$,*2*$^{flx/flx}$ MEFs where *Mfn1* and *Mfn2* were acutely ablated by Cre-recombinase delivered by viral infection or by parasite-derived secretion (Figures 7E, S7F, and S7G) (Koshy et al., 2010). Notably, the CPT1 inhibitor etomoxir promoted *Toxoplasma* proliferation in *Mfn1*$^{+/+}$,*2*$^{+/+}$ but not in *Mfn1*$^{-/-}$,*2*$^{-/-}$ MEFs (Figure 7E). Reintroduction of *Mfn1* required for mitochondrial FA uptake from LDs (Rambold et al., 2015) partially restricted parasite growth in *Mfn1*$^{-/-}$,*2*$^{-/-}$ MEFs (Figure 7F). These results support a model in which mitochondrial fusion enhances FAO, limiting parasite access to host FAs and ultimately restricting its growth.

DISCUSSION

A key aspect of the host-pathogen interaction is the scavenging of host nutrients by microbes. Pathogens have therefore evolved strategies to extract host metabolites, and the host cell has developed countermeasures. Here we demonstrate that while a pathogen can co-opt host lipophagy to gain access to intracellular lipid stores, host mitochondria fuse around the pathogen vacuole to competitively take up FAs, limiting the parasite access to a key host resource and thereby restricting its growth.

Although our work focused on *Toxoplasma*, a protozoan parasite, the competition between host organelles and pathogens for limited nutrients is a conceptual framework generalizable to most intracellular infections. This competition encompasses pathogen exploitation of metabolic processes, such as host proteasomal degradation for access to amino acids, and host autophagy for access to a range of metabolites including amino acids, as during *Francisella* infection (Steele et al., 2015), and FAs as we demonstrate here. In addition to FAs, host autophagy might provide *Toxoplasma* access to a broad range of nutrients,

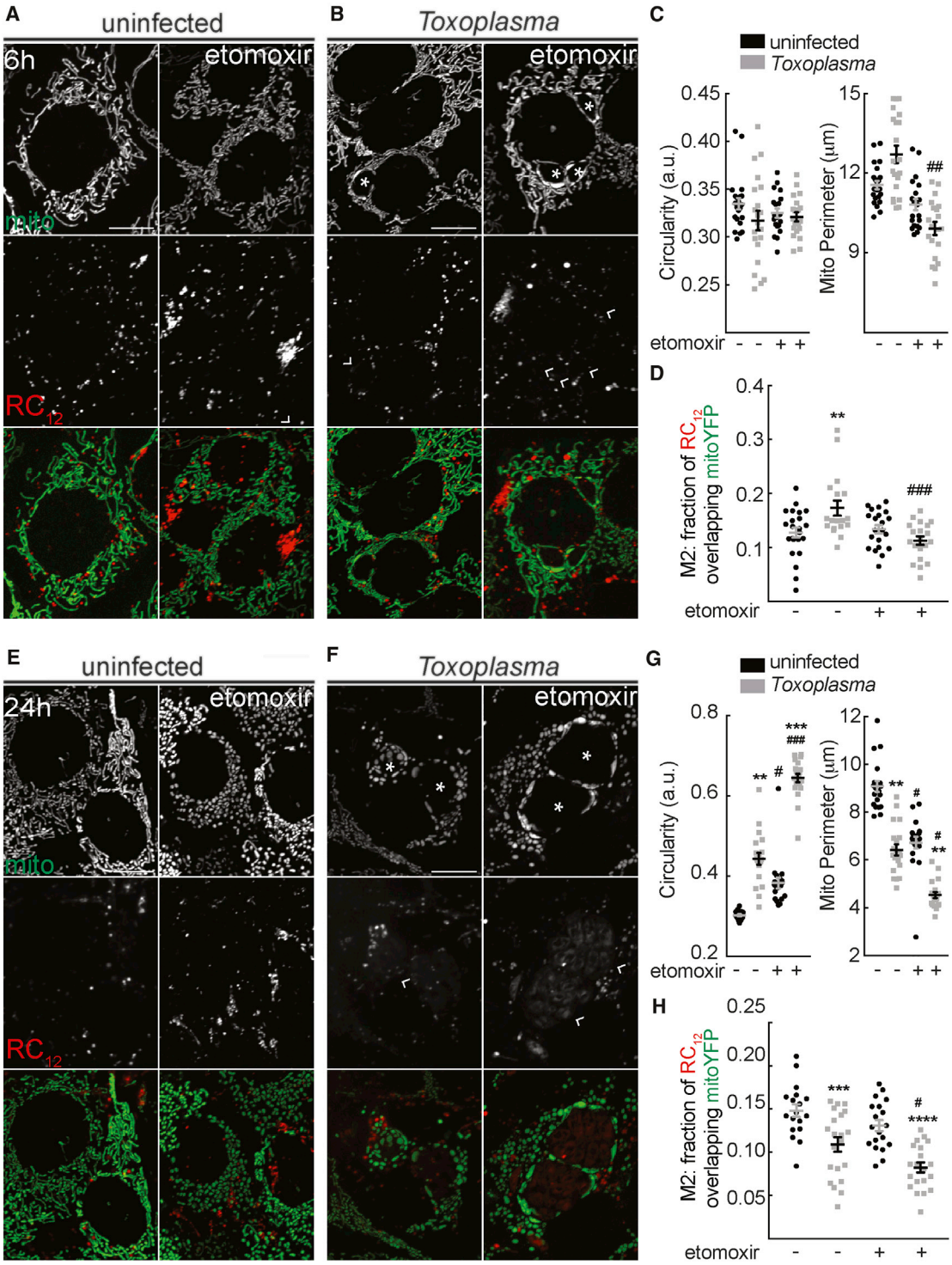

Figure 6. Early Mitochondrial FA Uptake during *Toxoplasma* Infection Limits Parasite Proliferation

(A and B) Where indicated, MEFs expressing mtYFP incubated with RC_{12} overnight were infected with *Toxoplasma*. Cells were rinsed and at 2 hpi treated where indicated with etomoxir, and 6 hpi confocal z stacks of mtYFP and RC_{12} were acquired. Parasite vacuoles are indicated by asterisks (mitoYFP panel) and arrowheads (RC_{12} panel). Scale bar, 10 μm.

(C) Average perimeter and circularity analysis of mitochondria in uninfected cells (A) and infected cells (B). Data are mean ± SEM of n = 20 fields (>200 cells for uninfected, >30 cells for *Toxoplasma*-infected cells). $^{\#\#}p < 0.01$, untreated versus etomoxir-treated by two-way ANOVA.

(D) Fraction of RC_{12} overlapping mitoYFP in experiments as in (A) and (B). Data are mean ± SEM of n = 20 fields (>200 cells for uninfected, >30 cells for *Toxoplasma*-infected cells). $^{**}p < 0.01$ uninfected versus *Toxoplasma*-infected, $^{\#\#\#}p < 0.001$ untreated versus chloroquine-treated by two-way ANOVA.

(legend continued on next page)

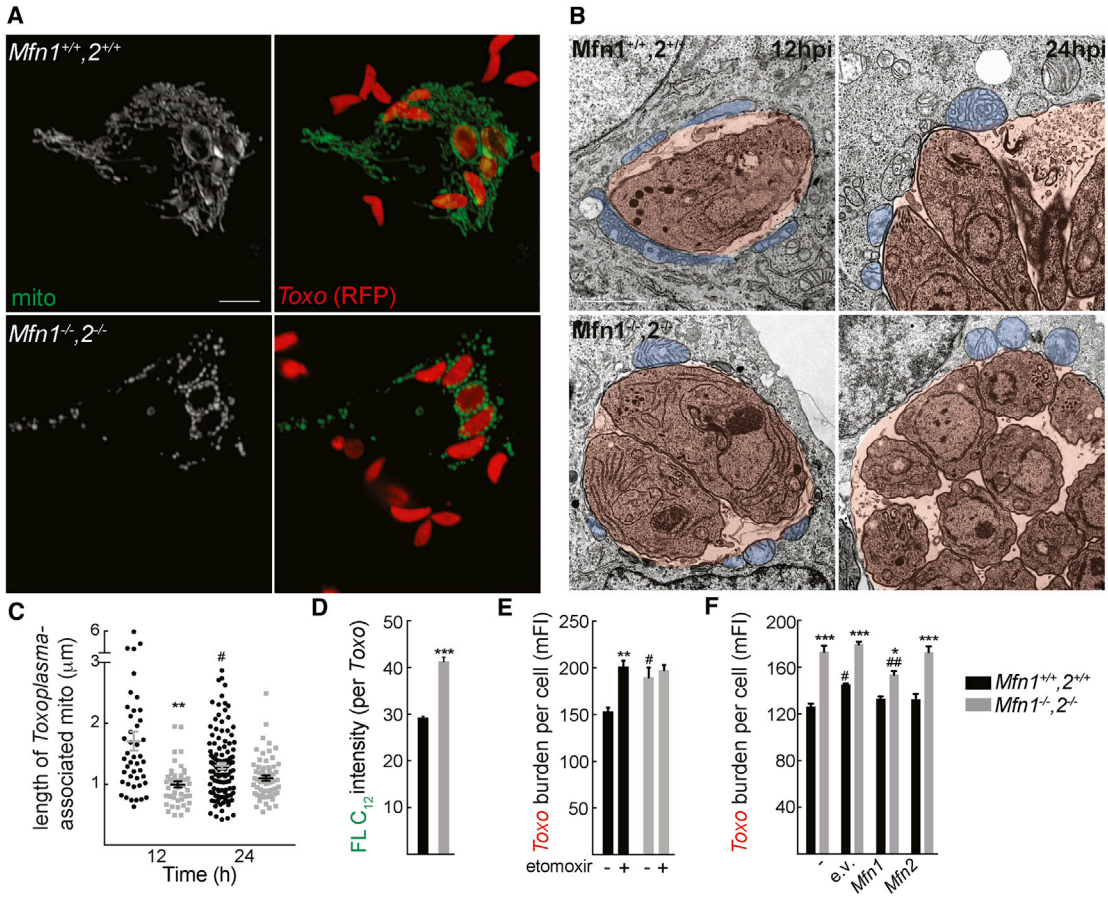

Figure 7. Host Mitochondrial Fusion Restricts *Toxoplasma* Proliferation

(A) z stack projections of confocal images of MEFs of the indicated genotype expressing mtYFP and imaged at 6 hpi with *RFP*$^{+}$-*Toxoplasma* parasites. Scale bar, 10 μm.

(B) EM analysis of *Toxoplasma* vacuoles and associated host mitochondria in MEFs of the indicated genotype at the indicated times. *Toxoplasma* vacuoles are shaded in red and mitochondria in blue. Scale bar, 2 μm.

(C) Morphometric analysis of length of *Toxoplasma*-associated mitochondria in experiments as in (B). Data are mean ± SEM from n = 40 EMs, $^{**}p < 0.01$ for *Mfn1*$^{+/+}$,*2*$^{+/+}$ versus *Mfn1*$^{+/+}$,*2*$^{+/+}$, $^{\#}p < 0.01$ for 12 hr versus 24 hr by two-way ANOVA.

(D) Flow cytometry analysis of FL C_{12} MFI of *RFP*$^{+}$-*Toxoplasma* isolated from FL C_{12}-pulsed MEFs of the indicated genotype. Data are mean + SEM from n = 3 independent experiments, $^{***}p < 0.001$ by unpaired t test.

(E) MEFs of the indicated genotype were infected with *RFP*$^{+}$-*Toxoplasma* (MOI = 2), rinsed at 2 hpi, and incubated in complete medium supplemented where indicated with etomoxir and analyzed by flow cytometry for *Toxoplasma* burden (RFP mFI). Data are mean + SEM of n = 3 experiments, $^{**}p < 0.01$ for treated versus untreated, $^{\#}p < 0.05$ for *Mfn1*$^{+/+}$,*2*$^{+/+}$ and *Mfn1*$^{-/-}$,*2*$^{-/-}$ MEFs by two-way ANOVA.

(F) MEFs of the indicated genotype transfected as indicated were infected with *RFP*$^{+}$-*Toxoplasma* (MOI = 2), replaced with complete medium at 2 hpi and analyzed by flow cytometry for *Toxoplasma* burden (RFP mFI) at 24 hpi. Data are mean + SEM of n = 3 experiments, $^{*}p < 0.01$, $^{***}p < 0.0001$ for *Mfn1*$^{+/+}$,*2*$^{+/+}$ versus *Mfn1*$^{-/-}$,*2*$^{-/-}$; $^{\#}p < 0.05$, $^{\#\#}p < 0.01$ for *Mfn1* or *Mfn2* expression versus e.v. by two-way ANOVA.

For (C) to (F), black indicates *Mfn1*$^{+/+}$,*2*$^{+/+}$ and gray indicates *Mfn1*$^{-/-}$,*2*$^{-/-}$, as bottom right legend indicates. See also Figure S7.

ranging from nucleosides to sterols, given that the addition of FA linoleate and oleate only partially complemented parasite growth in cells lacking autophagy.

It is likely that the competition for nutrients between mitochondria and *Toxoplasma* extends beyond FA: these organelles also oxidize pyruvate and amino acids, and

(E and F) Where indicated, MEFs expressing mtYFP incubated with RC_{12} overnight were infected with *Toxoplasma*. Cells were rinsed and at 2 hpi treated where indicated with etomoxir, and 24 hpi confocal z stacks of mtYFP and RC_{12} were acquired. Parasite vacuoles are indicated by asterisks (mitoYFP panel) and arrowheads (RC_{12} panel). Scale bar, 10 μm.

(G) Average perimeter and circularity analysis of mitochondria in uninfected cells (E) and infected cells (F). Data are mean ± SEM of n = 20 (>200 cells for uninfected, >30 cells for *Toxoplasma*-infected cells). $^{**}p < 0.01$, $^{***}p < 0.001$ uninfected versus *Toxoplasma*-infected, $^{\#}p < 0.05$, $^{\#\#\#}p < 0.001$ untreated versus etomoxir-treated by two-way ANOVA.

(H) Fraction of RC_{12} overlapping mitoYFP in experiments as in (A) and (B). Data are mean ± SEM of n = 20 (>200 cells for uninfected, >30 cells for *Toxoplasma*-infected cells). $^{***}p < 0.001$, $^{****}p < 0.0001$ uninfected versus *Toxoplasma*-infected, $^{\#}p < 0.05$ untreated versus etomoxir-treated by two-way ANOVA.

See also Figure S6.

participate in one-carbon metabolism essential for anabolic pathways. Host organelles that can compete for nutrients with pathogens might include the ER and LDs (both FA and sterol depots), which also traffic to vacuoles surrounding other pathogens (Dumoux and Hayward, 2016; Peyron et al., 2008).

The discovery that the mitochondrial antiviral signaling protein (MAVS) must be obligatorily localized on mitochondrial outer membrane to activate the antiviral response leading to type I interferons and proinflammatory cytokine production cemented the role of mitochondria as signaling hubs in innate immunity (Kawai et al., 2005; Meylan et al., 2005; Seth et al., 2005; Xu et al., 2005). Our work provides a second paradigm by which mitochondria participate in innate immunity: they mount a "metabolic defense" against *Toxoplasma* infection through sequestration of FAs, for which mitochondrial fusion is required. Thus, it is no surprise that microbes have evolved diverse strategies to influence mitochondrial dynamics: *V. cholerae* modulates mitochondrial trafficking (Suzuki et al., 2014); mitochondrial fission is often observed in infected cells, being caused by a secreted toxin, as in the case of *Listeria monocytogenes* (Stavru et al., 2011) or by an effector protein in the case of *L. pneumophila* (Escoll et al., 2017). Conversely and unexpectedly, the bacterium *Chlamydia trachomatis* benefits from preserving the host mitochondrial network (Chowdhury et al., 2017). It will be interesting to address whether the formation of contact sites between certain microbes such as *Toxoplasma* and mitochondria (Dumoux and Hayward, 2016; Onoguchi et al., 2010; Sinai et al., 1997) represents a generalized strategy to obstruct the type of metabolic innate immunity described here.

Our results reveal another layer of mitochondrial involvement in innate immunity. Mitochondria, by fusing and taking up FAs, can defend host cells against infection by sequestering nutrients from an intracellular parasite. The framework of competition between microbes and host cells for non-diffusible metabolites opens the possibility for therapeutic strategies that modulate host metabolism to limit pathogen access to nutrients and ultimately control infection.

Limitations of Study

Because of the intimate relationship between mitochondrial form and function, we cannot exclude that the mitochondrial elongation and enhanced FA uptake observed following infection are a consequence of the high energetic demand of infection with an intracellular pathogen that scavenges a wide variety of metabolites from its host (Tymoshenko et al., 2015). Another limitation of our study lies in the nature of the metabolites for which mitochondria and *Toxoplasma* compete: we cannot exclude that part of the observed effect of mitochondrial elongation against parasite growth is due to, e.g., amino acids or pyruvate scavenging. Accumulation of acylcarnitines following etomoxir inhibition of carnitine-palmitoyl transferase might lead to lipotoxicity (Nguyen et al., 2017), thereby increasing *Toxoplasma* growth. Genetic models deficient for cellular starvation response regulators and for mitochondrial FAO are necessary to dissect the relative contribution of these different host processes in limiting infection by an intracellular pathogen.

STAR★METHODS

Detailed methods are provided in the online version of this paper and include the following:

- KEY RESOURCES TABLE
- CONTACT FOR REAGENT AND RESOURCE SHARING
- EXPERIMENTAL MODEL AND SUBJECT DETAILS
  - Cell Culture
  - Subcutaneous Adipose Tissue Isolation
- METHOD DETAILS
  - Electron Microscopy
  - Plasmid Design and Construction
  - Molecular Biology
  - Biochemistry
  - Cell Line Generation
  - Parasite Culture and Strains
  - Confocal Microscopy
  - Counting of LC3-PLIN3 Puncta
  - Pulse-Chase Experiments
  - Flow Cytometry Analysis of Parasites
  - Flow Cytometry Analysis of Infection
  - Plaque Assay
- QUANTIFICATION AND STATISTICAL ANALYSIS

SUPPLEMENTAL INFORMATION

Supplemental Information includes seven figures and can be found with this article online at https://doi.org/10.1016/j.cmet.2018.02.018.

ACKNOWLEDGMENTS

We thank Drs. F. Caicci and F. Boldrin (EM facility, Department of Biology, University of Padova) for EM sample preparation, Dr. M. Giacomello (Department of Biology, University of Padova) for help with confocal microscopy, Dr. A. Cabrelle (Flow Cytometry facility, VIMM) for support in FACS analysis, and D. Pernas and S. Pernas for critical reading of the manuscript. L.P. was supported by an EMBO Long Term Postdoctoral and a DTI-IMPORT FP7 Fellowship and is supported by a Simons Foundation-Life Science Research Fellowship. This work was supported by NIH RO1 AI073756 to J.C.B., ERC FP7-282280 and FP7 CIG PCIG13-GA-2013-618697, Italian Ministry of Research FIRB RBAP11Z3YA_005, and an EFSD/Novo Nordisk Program for Diabetes Research in Europe grant to L.S.

AUTHOR CONTRIBUTIONS

L.P. and L.S. conceived the project and wrote the manuscript. L.P. performed and analyzed experiments. C.B. isolated primary adipocytes. J.B. advised and edited the manuscript. L.S. supervised the project.

DECLARATION OF INTERESTS

The authors declare no competing interests.

Received: July 22, 2017
Revised: January 5, 2018
Accepted: February 20, 2018
Published: April 3, 2018

REFERENCES

Abu Kwaik, Y., and Bumann, D. (2015). Host delivery of favorite meals for intracellular pathogens. PLoS Pathog. *11*, e1004866.

Andrade, R.M., Wessendarp, M., Gubbels, M.J., Striepen, B., and Subauste, C.S. (2006). CD40 induces macrophage anti-*Toxoplasma gondii* activity by

triggering autophagy-dependent fusion of pathogen-containing vacuoles and lysosomes. J. Clin. Invest. *116*, 2366–2377.

Black, M.W., and Boothroyd, J.C. (2000). Lytic cycle of *Toxoplasma gondii*. Microbiol. Mol. Biol. Rev. *64*, 607–623.

Brieland, J.K., Fantone, J.C., Remick, D.G., LeGendre, M., McClain, M., and Engleberg, N.C. (1997). The role of *Legionella pneumophila*-infected *Hartmannella vermiformis* as an infectious particle in a murine model of Legionnaire's disease. Infect. Immun. *65*, 5330–5333.

Caffaro, C.E., and Boothroyd, J.C. (2011). Evidence for host cells as the major contributor of lipids in the intravacuolar network of *Toxoplasma*-infected cells. Eukaryot. Cell *10*, 1095–1099.

Charron, A.J., and Sibley, L.D. (2002). Host cells: mobilizable lipid resources for the intracellular parasite *Toxoplasma gondii*. J. Cell Sci. *115*, 3049–3059.

Chen, H., Detmer, S.A., Ewald, A.J., Griffin, E.E., Fraser, S.E., and Chan, D.C. (2003). Mitofusins Mfn1 and Mfn2 coordinately regulate mitochondrial fusion and are essential for embryonic development. J. Cell Biol. *160*, 189–200.

Chowdhury, S.R., Reimer, A., Sharan, M., Kozjak-Pavlovic, V., Eulalio, A., Prusty, B.K., Fraunholz, M., Karunakaran, K., and Rudel, T. (2017). *Chlamydia* preserves the mitochondrial network necessary for replication via microRNA-dependent inhibition of fission. J. Cell Biol. *216*, 1071–1089.

Cipolat, S., Martins de Brito, O., Dal Zilio, B., and Scorrano, L. (2004). OPA1 requires mitofusin 1 to promote mitochondrial fusion. Proc. Natl. Acad. Sci. USA *101*, 15927–15932.

Cocchiaro, J.L., Kumar, Y., Fischer, E.R., Hackstadt, T., and Valdivia, R.H. (2008). Cytoplasmic lipid droplets are translocated into the lumen of the *Chlamydia trachomatis* parasitophorous vacuole. Proc. Natl. Acad. Sci. USA *105*, 9379–9384.

Coppens, I., Sinai, A.P., and Joiner, K.A. (2000). *Toxoplasma gondii* exploits host low-density lipoprotein receptor-mediated endocytosis for cholesterol acquisition. J. Cell Biol. *149*, 167–180.

Currie, E., Schulze, A., Zechner, R., Walther, T.C., and Farese, R.V., Jr. (2013). Cellular fatty acid metabolism and cancer. Cell Metab. *18*, 153–161.

Deretic, V. (2011). Autophagy in immunity and cell-autonomous defense against intracellular microbes. Immunol. Rev. *240*, 92–104.

Derouin, F., and Chastang, C. (1989). In vitro effects of folate inhibitors on *Toxoplasma gondii*. Antimicrob. Agents Chemother. *33*, 1753–1759.

Dumoux, M., and Hayward, R.D. (2016). Membrane contact sites between pathogen-containing compartments and host organelles. Biochim. Biophys. Acta *1861*, 895–899.

Escoll, P., Song, O.R., Viana, F., Steiner, B., Lagache, T., Olivo-Marin, J.C., Impens, F., Brodin, P., Hilbi, H., and Buchrieser, C. (2017). *Legionella pneumophila* modulates mitochondrial dynamics to trigger metabolic repurposing of infected macrophages. Cell Host Microbe *22*, 302–316.e7.

Farese, R.V., Jr., and Walther, T.C. (2009). Lipid droplets finally get a little R-E-S-P-E-C-T. Cell *139*, 855–860.

Favaretto, F., Milan, G., Collin, G.B., Marshall, J.D., Stasi, F., Maffei, P., Vettor, R., and Naggert, J.K. (2014). GLUT4 defects in adipose tissue are early signs of metabolic alterations in Alms1GT/GT, a mouse model for obesity and insulin resistance. PLoS One *9*, e109540.

Fox, B.A., Gigley, J.P., and Bzik, D.J. (2004). *Toxoplasma gondii* lacks the enzymes required for de novo arginine biosynthesis and arginine starvation triggers cyst formation. Int. J. Parasitol. *34*, 323–331.

Friis, R.R. (1972). Interaction of L cells and *Chlamydia psittaci*: entry of the parasite and host responses to its development. J. Bacteriol. *110*, 706–721.

Fujimoto, Y., Onoduka, J., Homma, K.J., Yamaguchi, S., Mori, M., Higashi, Y., Makita, M., Kinoshita, T., Noda, J., Itabe, H., et al. (2006). Long-chain fatty acids induce lipid droplet formation in a cultured human hepatocyte in a manner dependent of Acyl-CoA synthetase. Biol. Pharm. Bull. *29*, 2174–2180.

Gao, D., Zhang, J., Zhao, J., Wen, H., Pan, J., Zhang, S., Fang, Y., Li, X., Cai, Y., Wang, X., et al. (2014). Autophagy activated by *Toxoplasma gondii* infection in turn facilitates Toxoplasma gondii proliferation. Parasitol. Res. *113*, 2053–2058.

Gomes, L.C., Di Benedetto, G., and Scorrano, L. (2011). During autophagy mitochondria elongate, are spared from degradation and sustain cell viability. Nat. Cell Biol. *13*, 589–598.

Hacker, C., Howell, M., Bhella, D., and Lucocq, J. (2014). Strategies for maximizing ATP supply in the microsporidian *Encephalitozoon cuniculi*: direct binding of mitochondria to the parasitophorous vacuole and clustering of the mitochondrial porin VDAC. Cell Microbiol. *16*, 565–579.

Harris, C.A., Haas, J.T., Streeper, R.S., Stone, S.J., Kumari, M., Yang, K., Han, X., Brownell, N., Gross, R.W., Zechner, R., et al. (2011). DGAT enzymes are required for triacylglycerol synthesis and lipid droplets in adipocytes. J. Lipid Res. *52*, 657–667.

Herms, A., Bosch, M., Reddy, B.J., Schieber, N.L., Fajardo, A., Ruperez, C., Fernandez-Vidal, A., Ferguson, C., Rentero, C., Tebar, F., et al. (2015). AMPK activation promotes lipid droplet dispersion on detyrosinated microtubules to increase mitochondrial fatty acid oxidation. Nat. Commun. *6*, 7176.

Horwitz, M.A. (1983). Formation of a novel phagosome by the Legionnaires' disease bacterium (*Legionella pneumophila*). J. Exp. Med. *158*, 1319–1331.

Jones, T.C., and Hirsch, J.G. (1972). The interaction between Toxoplasma gondii and mammalian cells. II. The absence of lysosomal fusion with phagocytic vacuoles containing living parasites. J. Exp. Med. *136*, 1173–1194.

Kawai, T., Takahashi, K., Sato, S., Coban, C., Kumar, H., Kato, H., Ishii, K.J., Takeuchi, O., and Akira, S. (2005). IPS-1, an adaptor triggering RIG-I- and Mda5-mediated type I interferon induction. Nat. Immunol. *6*, 981–988.

Kofoed, E.M., and Vance, R.E. (2011). Innate immune recognition of bacterial ligands by NAIPs determines inflammasome specificity. Nature *477*, 592–595.

Komatsu, M., Waguri, S., Ueno, T., Iwata, J., Murata, S., Tanida, I., Ezaki, J., Mizushima, N., Ohsumi, Y., Uchiyama, Y., et al. (2005). Impairment of starvation-induced and constitutive autophagy in Atg7-deficient mice. J. Cell Biol. *169*, 425–434.

Koshy, A.A., Fouts, A.E., Lodoen, M.B., Alkan, O., Blau, H.M., and Boothroyd, J.C. (2010). Toxoplasma secreting Cre recombinase for analysis of host-parasite interactions. Nat. Methods *7*, 307–309.

Late de Late, P., Pineda, M., Harnett, M., Harnett, W., Besteiro, S., and Langsley, G. (2017). Apicomplexan autophagy and modulation of autophagy in parasite-infected host cells. Biomed. J. *40*, 23–30.

Leanza, L., Romio, M., Becker, K.A., Azzolini, M., Trentin, L., Manago, A., Venturini, E., Zaccagnino, A., Mattarei, A., Carraretto, L., et al. (2017). Direct pharmacological targeting of a mitochondrial ion channel selectively kills tumor cells in vivo. Cancer Cell *31*, 516–531.e10.

Lopaschuk, G.D., Wall, S.R., Olley, P.M., and Davies, N.J. (1988). Etomoxir, a carnitine palmitoyltransferase I inhibitor, protects hearts from fatty acid-induced ischemic injury independent of changes in long chain acylcarnitine. Circ. Res. *63*, 1036–1043.

Mayer, N., Schweiger, M., Romauch, M., Grabner, G.F., Eichmann, T.O., Fuchs, E., Ivkovic, J., Heier, C., Mrak, I., Lass, A., et al. (2013). Development of small-molecule inhibitors targeting adipose triglyceride lipase. Nat. Chem. Biol. *9*, 785–787.

Meylan, E., Curran, J., Hofmann, K., Moradpour, D., Binder, M., Bartenschlager, R., and Tschopp, J. (2005). Cardif is an adaptor protein in the RIG-I antiviral pathway and is targeted by hepatitis C virus. Nature *437*, 1167–1172.

Montoya, J.G., and Liesenfeld, O. (2004). Toxoplasmosis. Lancet *363*, 1965–1976.

Mota, L.A., Roberto Neto, J., Monteiro, V.G., Lobato, C.S., Oliveira, M.A., Cunha, M., D'Avila, H., Seabra, S.H., Bozza, P.T., and DaMatta, R.A. (2014). Culture of mouse peritoneal macrophages with mouse serum induces lipid bodies that associate with the parasitophorous vacuole and decrease their microbicidal capacity against *Toxoplasma gondii*. Mem. Inst. Oswaldo Cruz *109*, 767–774.

Naon, D., Zaninello, M., Giacomello, M., Varanita, T., Grespi, F., Lakshminaranayan, S., Serafini, A., Semenzato, M., Herkenne, S., Hernandez-Alvarez, M.I., et al. (2016). Critical reappraisal confirms that Mitofusin 2 is an endoplasmic reticulum-mitochondria tether. Proc. Natl. Acad. Sci. USA *113*, 11249–11254.

Nguyen, T.B., Louie, S.M., Daniele, J.R., Tran, Q., Dillin, A., Zoncu, R., Nomura, D.K., and Olzmann, J.A. (2017). DGAT1-dependent lipid droplet biogenesis protects mitochondrial function during starvation-induced autophagy. Dev. Cell *42*, 9–21.e5.

Nolan, S.J., Romano, J.D., and Coppens, I. (2017). Host lipid droplets: an important source of lipids salvaged by the intracellular parasite *Toxoplasma gondii*. PLoS Pathog. *13*, e1006362.

Onoguchi, K., Onomoto, K., Takamatsu, S., Jogi, M., Takemura, A., Morimoto, S., Julkunen, I., Namiki, H., Yoneyama, M., and Fujita, T. (2010). Virus-infection or 5'ppp-RNA activates antiviral signal through redistribution of IPS-1 mediated by MFN1. PLoS Pathog. *6*, e1001012.

Patten, D.A., Wong, J., Khacho, M., Soubannier, V., Mailloux, R.J., Pilon-Larose, K., MacLaurin, J.G., Park, D.S., McBride, H.M., Trinkle-Mulcahy, L., et al. (2014). OPA1-dependent cristae modulation is essential for cellular adaptation to metabolic demand. EMBO J. *33*, 2676–2691.

Pernas, L., Adomako-Ankomah, Y., Shastri, A.J., Ewald, S.E., Treeck, M., Boyle, J.P., and Boothroyd, J.C. (2014). Toxoplasma effector MAF1 mediates recruitment of host mitochondria and impacts the host response. PLoS Biol. *12*, e1001845.

Pernas, L., and Scorrano, L. (2016). Mito-morphosis: mitochondrial fusion, fission, and cristae remodeling as key mediators of cellular function. Annu. Rev. Physiol. *78*, 505–531.

Peyron, P., Vaubourgeix, J., Poquet, Y., Levillain, F., Botanch, C., Bardou, F., Daffe, M., Emile, J.F., Marchou, B., Cardona, P.J., et al. (2008). Foamy macrophages from tuberculous patients' granulomas constitute a nutrient-rich reservoir for *M. tuberculosis* persistence. PLoS Pathog. *4*, e1000204.

Rabhi, S., Rabhi, I., Trentin, B., Piquemal, D., Regnault, B., Goyard, S., Lang, T., Descoteaux, A., Enninga, J., and Guizani-Tabbane, L. (2016). Lipid droplet formation, their localization and dynamics during *Leishmania major* macrophage infection. PLoS One *11*, e0148640.

Ramakrishnan, S., Docampo, M.D., Macrae, J.I., Pujol, F.M., Brooks, C.F., van Dooren, G.G., Hiltunen, J.K., Kastaniotis, A.J., McConville, M.J., and Striepen, B. (2012). Apicoplast and endoplasmic reticulum cooperate in fatty acid biosynthesis in apicomplexan parasite *Toxoplasma gondii*. J. Biol. Chem. *287*, 4957–4971.

Ramakrishnan, S., Docampo, M.D., MacRae, J.I., Ralton, J.E., Rupasinghe, T., McConville, M.J., and Striepen, B. (2015). The intracellular parasite Toxoplasma gondii depends on the synthesis of long-chain and very long-chain unsaturated fatty acids not supplied by the host cell. Mol. Microbiol. *97*, 64–76.

Rambold, A.S., Cohen, S., and Lippincott-Schwartz, J. (2015). Fatty acid trafficking in starved cells: regulation by lipid droplet lipolysis, autophagy, and mitochondrial fusion dynamics. Dev. Cell *32*, 678–692.

Rambold, A.S., Kostelecky, B., Elia, N., and Lippincott-Schwartz, J. (2011). Tubular network formation protects mitochondria from autophagosomal degradation during nutrient starvation. Proc. Natl. Acad. Sci. USA *108*, 10190–10195.

Reggiori, F., and Klionsky, D.J. (2002). Autophagy in the eukaryotic cell. Eukaryot. Cell *1*, 11–21.

Rizk, A., Paul, G., Incardona, P., Bugarski, M., Mansouri, M., Niemann, A., Ziegler, U., Berger, P., and Sbalzarini, I.F. (2014). Segmentation and quantification of subcellular structures in fluorescence microscopy images using Squassh. Nat. Protoc. *9*, 586–596.

Rohwedder, A., Zhang, Q., Rudge, S.A., and Wakelam, M.J. (2014). Lipid droplet formation in response to oleic acid in Huh-7 cells is mediated by the fatty acid receptor FFAR4. J. Cell Sci. *127*, 3104–3115.

Romano, J.D., Sonda, S., Bergbower, E., Smith, M.E., and Coppens, I. (2013). Toxoplasma gondii salvages sphingolipids from the host Golgi through the rerouting of selected Rab vesicles to the parasitophorous vacuole. Mol. Biol. Cell *24*, 1974–1995.

Schindelin, J., Arganda-Carreras, I., Frise, E., Kaynig, V., Longair, M., Pietzsch, T., Preibisch, S., Rueden, C., Saalfeld, S., Schmid, B., et al. (2012). Fiji: an open-source platform for biological-image analysis. Nat. Methods *9*, 676–682.

Seth, R.B., Sun, L., Ea, C.K., and Chen, Z.J. (2005). Identification and characterization of MAVS, a mitochondrial antiviral signaling protein that activates NF-kappaB and IRF 3. Cell *122*, 669–682.

Sinai, A.P., Webster, P., and Joiner, K.A. (1997). Association of host cell endoplasmic reticulum and mitochondria with the *Toxoplasma gondii* parasitophorous vacuole membrane: a high affinity interaction. J. Cell Sci. *110*, 2117–2128.

Singh, R., Kaushik, S., Wang, Y., Xiang, Y., Novak, I., Komatsu, M., Tanaka, K., Cuervo, A.M., and Czaja, M.J. (2009). Autophagy regulates lipid metabolism. Nature *458*, 1131–1135.

Sonda, S., Ting, L.M., Novak, S., Kim, K., Maher, J.J., Farese, R.V., Jr., and Ernst, J.D. (2001). Cholesterol esterification by host and parasite is essential for optimal proliferation of *Toxoplasma gondii*. J. Biol. Chem. *276*, 34434–34440.

Song, M., Mihara, K., Chen, Y., Scorrano, L., and Dorn, G.W., 2nd (2015). Mitochondrial fission and fusion factors reciprocally orchestrate mitophagic culling in mouse hearts and cultured fibroblasts. Cell Metab. *21*, 273–285.

Souto, X.M., Barbosa, H.S., and Menna-Barreto, R.F. (2016). The morphological analysis of autophagy in primary skeletal muscle cells infected with *Toxoplasma gondii*. Parasitol. Res. *115*, 2853–2861.

Stavru, F., Bouillaud, F., Sartori, A., Ricquier, D., and Cossart, P. (2011). *Listeria monocytogenes* transiently alters mitochondrial dynamics during infection. Proc. Natl. Acad. Sci. USA *108*, 3612–3617.

Steele, S., Brunton, J., and Kawula, T. (2015). The role of autophagy in intracellular pathogen nutrient acquisition. Front. Cell. Infect. Microbiol. *5*, 51.

Suzuki, M., Danilchanka, O., and Mekalanos, J.J. (2014). *Vibrio cholerae* T3SS effector VopE modulates mitochondrial dynamics and innate immune signaling by targeting Miro GTPases. Cell Host Microbe *16*, 581–591.

Syn, G., Anderson, D., Blackwell, J.M., and Jamieson, S.E. (2017). *Toxoplasma gondii* infection is associated with mitochondrial dysfunction in-vitro. Front. Cell. Infect. Microbiol. *7*, 512.

Sznaidman, M.L., Haffner, C.D., Maloney, P.R., Fivush, A., Chao, E., Goreham, D., Sierra, M.L., LeGrumelec, C., Xu, H.E., Montana, V.G., et al. (2003). Novel selective small molecule agonists for peroxisome proliferator-activated receptor delta (PPARdelta)—synthesis and biological activity. Bioorg. Med. Chem. Lett. *13*, 1517–1521.

Tymoshenko, S., Oppenheim, R.D., Agren, R., Nielsen, J., Soldati-Favre, D., and Hatzimanikatis, V. (2015). Metabolic needs and capabilities of *Toxoplasma gondii* through combined computational and experimental analysis. PLoS Comput. Biol. *11*, e1004261.

Walther, T.C., and Farese, R.V., Jr. (2012). Lipid droplets and cellular lipid metabolism. Annu. Rev. Biochem. *81*, 687–714.

Wang, Y., Weiss, L.M., and Orlofsky, A. (2009). Host cell autophagy is induced by *Toxoplasma gondii* and contributes to parasite growth. J. Biol. Chem. *284*, 1694–1701.

Xu, L.G., Wang, Y.Y., Han, K.J., Li, L.Y., Zhai, Z., and Shu, H.B. (2005). VISA is an adapter protein required for virus-triggered IFN-beta signaling. Mol. Cell *19*, 727–740.

STAR★METHODS

KEY RESOURCES TABLE

REAGENT or RESOURCE	SOURCE	IDENTIFIER
Antibodies		
Rabbit monoclonal anti-LC3	Novus	NB100-2331 (LC3); RRID: AB_1109173
Mouse anti-y-tubulin	Sigma	T6557 (Tubulin); RRID: AB_477584
Rabbit polyclonal anti-GAPDH	Sigma	G9545; RRID: AB_1078992
Mouse polyclonal anti-MAF1	(Pernas et al., 2014)	N/A
Amersham ECL Rabbit IgG, HRP-linked whole Ab	GE Healthcare Life Sci	NA934
Amersham ECL Mouse IgG, HRP-linked whole Ab	GE Healthcare Life Sci	NA931
Bacterial and Virus Strains		
pMSCV-eGFP	Addgene	91975
pMSCV-Cre-eGFP	Addgene	24064
pMSCV2.2	(Kofoed and Vance, 2011)	60206
pMSCV2.2/Mfn1	This paper	N/A
pMSCV2.2/Mfn2	This paper	N/A
Chemicals, Peptides, and Recombinant Proteins		
Pyrimethamine	Sigma-Aldrich	46706
MitoTEMPO	Sigma-Aldrich	SML0737
Etomoxir	Sigma-Aldrich	E1905
Atglistatin	Sigma-Aldrich	SML1075
Chloroquine diphosphate	Sigma-Aldrich	C6628
GW0742	Sigma-Aldrich	G3295
Critical Commercial Assays		
Pierce ECL Plus Western Blotting	Life Technologies	32132
TransFectin Lipid Reagent	BioRad	170-3352
Experimental Models: Cell Lines		
Human Foreskin Fibrolasts (HFFs)	ATCC	SCRC-1041
Primary Subcutaneous Mouse Adipose Tissue	This paper	N/A
Caco-2	ATCC	HTB-37
Wild-type murine embryonic fibroblasts (MEFs)	ATCC	CRL-2991
Mfn1$^{-/-}$,*2*$^{-/-}$ MEFs	ATCC	CRL-2994
Mfn1$^{-/-}$,*2*$^{-/-}$::Mfn1	This paper	N/A
Mfn1$^{-/-}$,*2*$^{-/-}$::Mfn2	This paper	N/A
Atg7$^{+/+}$ MEFs	Laboratory of Dr.M. Sandri	N/A
Atg7$^{-/-}$ MEFs	Laboratory of Dr. M. Sandri	N/A
Dgat1$^{+/+}$,*2*$^{+/+}$ MEFs	(Harris et al., 2011)	N/A
Dgat1$^{-/-}$,*2*$^{-/-}$ MEFs	(Harris et al., 2011)	N/A
Mfn1$^{flx/flx}$,*Mfn2*$^{flx/flx}$ MEFs	(Song et al., 2015)	N/A
Mfn1$^{flx/flx}$,*Mfn2*$^{flx/flx}$:GFP MEFs	This paper	N/A
Mfn1$^{flx/flx}$,*Mfn2*$^{flx/flx}$:CreGFP MEFs	This paper	N/A
Experimental Models: Organisms/Strains		
T. gondii: strain RHΔHXGPRT	ATCC	50838
T. gondii: strain RH/Δku80:RFP	(Pernas et al., 2014)	N/A
T. gondii: strain RH/HA-ToxofilinCre/(SeCreEt)	(Koshy et al., 2010)	N/A

(*Continued on next page*)

Continued

REAGENT or RESOURCE	SOURCE	IDENTIFIER
Oligonucleotides		
Mfn1_F:AA CTC GAG CAC C AT GGC AGA AAC GGT ATC TCC	This paper	N/A
Mfn2:FAA CTC GAG CAC CAT GTC CCT GCT CTT TTC TCG	This paper	N/A
MfnR:AA GCGGCCGC CTA CCC AAG CTT GGT ACC GAG C	This paper	N/A
Recombinant DNA		
eGFP-LC3B	Addgene, Laboratory of Karla Kirkegaard	#11546
pEYFP-Mito	Clontech	PT3263-5
pSV40	Addgene	#21826
Software and Algorithms		
JACoP	ImageJ	https://imagej.nih.gov/ij/plugins/track/jacop.html
Squashh	Rizk et al., 2014	https://imagej.net/Squassh
Prism, version 7.0	GraphPad	http://www.graphpad.com/
FIJI running ImageJ, version 2.0	(Schindelin et al., 2012)	http://imagej.net/Welcome
CellQuest Pro	BD Biosciences	http://www.bdbiosciences.com/
Other		
Linoleic Acid	Sigma-Aldrich	L1376
BODIPY 493/503	Thermo Fisher	D3922
BODIPY FL C_{12}	Thermo Fisher Scientific	D3822
BODIPY 558/568 C_{12}	Thermo Fisher Scientific	D3835
Synthechol NS0 Supplement	Sigma-Aldrich	S5442
Linoleic Acid-Oleic Acid-Albumin, 100x	Sigma-Aldrich	L9655

CONTACT FOR REAGENT AND RESOURCE SHARING

Further information and requests for resources and reagents should be directed to and will be fulfilled by the Lead Contact, Luca Scorrano (luca.scorrano@unipd.it). An MTA was acquired from Dr. R. Farese (Harvard Public School of Health) for *Dgat1*$^{+/+}$,*2*$^{+/+}$ and *Dgat1*$^{-/-}$,*2*$^{-/-}$ MEFs.

EXPERIMENTAL MODEL AND SUBJECT DETAILS

Cell Culture

Caco-2 human intestinal epithelial cells, Wt and *Mfn1*$^{-/-}$,*2*$^{-/-}$ mouse embryonic fibroblasts (MEFs) were obtained from ATCC (HTB-37, CRL-2991, CRL-2994, respectively). *Atg7*$^{-/-}$ MEFs were provided by Dr. M Sandri (University of Padua), *Dgat1*$^{-/-}$,*2*$^{-/-}$ MEFs by Dr. R. Farese (Harvard Public School of Health). Caco-2 cells and MEFs were cultured in complete DMEM (cDMEM: DMEM supplemented with sodium pyruvate, glutamine, with 10% heat-inactivated FBS, 100 U/ml penicillin, and 100 μg/ml streptomycin) at 37C.

Subcutaneous Adipose Tissue Isolation

Subcutaneous adipose tissue was isolated as described (Favaretto et al., 2014). Adipose tissue was digested in collagenase type II solution, centrifuged, and red blood cells were lysed. Cells from the stromal vascular fraction were seeded in DMEM F12 supplemented with 150 U/ml streptomycin, 200 U/ml penicillin, 2 mM glutamine, 1 mM HEPES and 10% FBS. At confluency, fresh DMEM F12 containing 66 nM insulin, 100 nM dexamethasone, 1 nM T3, 0.25 mM IBMX, 10 μM rosiglitazone and 5% FBS was added. IBMX and rosiglitazone were removed after 3 days of culture. After day 7, cells were cultured in DMEM F12.

METHOD DETAILS

Electron Microscopy

MEF monolayers were infected with *Toxoplasma* for 24h and fixed in 2.5% glutaraldehyde in 0.1 M sodium cacodylate pH 7.4. EMs were acquired as described. ImageJ was used to measure the length of the mitochondria closely associated with the parasite vacuole (<30nm) in electron micrographs.

Plasmid Design and Construction

To construct pMSCV2.2/Mfn1 and pMSCV2.2/Mfn2, cDNA of Mfn1 (Addgene, #23212) and Mfn2 (Addgene, #23213) (Chen et al., 2003) with C-termal myc tags were amplified (see Key Resources Table for oligonucleotides) and ligated into the XhoI and NotI sites of pMSCV2.2 (Addgene, #60206).

Molecular Biology

MEFs were transfected using Transfectin following manufacturer's instructions with LC3-GFP (Plasmid #11546, Addgene), Perilipin3-RFP (pTagRFP-C; a gift from D. Sabatini, MIT), and mtYFP (Cipolat et al., 2004).

Biochemistry

Cell lysate preparation and immunoblotting were performed as previously described (Pernas et al., 2014). The following antibodies were used: anti-LC3 (Novus NB100-2331), GADPH (Sigma-Aldrich) anti-y-tubulin (Sigma-Aldrich), and polyclonal anti-MAF1 sera (Pernas et al., 2014).

Cell Line Generation

Mfn1$^{flx/flx}$,*2*$^{flx/flx}$ MEFs (a gift from Dr. G.W. Dorn II, Washington University St. Louis) were generated as described (Naon et al., 2016) and immortalized by SV40 Large T antigen expression. For stable MFN1 and MFN2 expression in MEFs, the coding region for the full-length *Mfn1* and *Mfn2* with C-terminal myc-epitope tags were PCR-amplified and cloned into the XhoI and NotI sites of the MSCV2.2 vector (Addgene #60206) downstream of the CMV promoter. The forward primers included the Kozak consensus sequence (CACC) before the start codon.

Introduction of Cre-recombinase into *Mfn1*$^{flx/flx}$,*2*$^{flx/flx}$ cells was performed using pMSCV-Cre derived ecotropic retroviruses. Phoenix cells were transfected with 15 μg of the relevant vector using Transfectin (BioRad). 24h after transfection, the supernatant was removed and replaced with fresh cDMEM and the cells transferred to 32°C. The following day the supernatant was filtered with a 0.2 μm filter, and following the addition of polybrene at a concentration of 5 mg/ml, the mix was transferred to MEFs at a confluency of 50%. MEFs were incubated for one day at 32C and then returned to 37C for expansion. Cells positive for GFP-expression were FACS-isolated and cultured for subsequent experiments.

Parasite Culture and Strains

Toxoplasma gondii parasites of the Type I (RH*Δhxgprt*) strain (deleted for the hypoxanthine-xanthine-guanine phosphoribosyl transferase (*HXGPRT*) gene), Type I (RH*Δku80:RFP*), Type I (RH*Δku80:RFP*), and Type I SeCreEt strain (Koshy et al., 2010) were maintained by serial passage in human foreskin fibroblast (HFF) monolayers in complete DMEM supplemented with 2mM glutamine.

Confocal Microscopy

For lipid droplet imaging, confluent monolayers of indicated cell type were incubated with BODIPY493/503 (Thermo Fisher Scientific) at 500ng/ml in complete media for 30 minutes before imaging. Cells were imaged with a Leica TCS SP5 inverted confocal microscope using an HCX PL APO 40X oil objective /numerical aperture 1.25-0.75 at 100Hz and 488nm and 541nm lasers for excitation. Images were acquired by using the Leica AS software. LD number per cell was counted in merged brightfield and BODIPY images after processed in Fiji.

Counting of LC3-PLIN3 Puncta

MEFs were plated on glass coverslips in 24-well plates, transfected using Transfectin following manufacturer's instructions with LC3-GFP and Perilipin3-RFP. 12h following transfection, cells were mock-infected or infected with *Toxoplasma* at an MOI:3. Cells were fixed at 6, 12, and 24h after infection in prewarmed cDMEM containing 3.7% formaldehyde for 15 min and imaged using a Leica DFC425 camera with an automated Leica DM5000B microscope using a 100X oil immersion objective. Images were acquired using Leica Acquisition software. Merged images were counted for the number of structures in which LC3 labeled puncta were adjacent to PLIN3 puncta.

Pulse-Chase Experiments

MEFs were plated on glass coverslips in 24-well plates (for observation after fixation) or CellView cell culture dishes (Greiner Bio-One) with a glass bottom (for live imaging) and labeled with 1μM of the indicated fluorescent fatty acid (BODIPY FL C_{12} or BODIPY 558/568 C_{12}, Thermo Fisher Scientific) overnight in cDMEM. MEF monolayers were rinsed twice with prewarmed 1X Hank's Balanced Salt Solution and then treated with mock media (syringe-lysed HFFs) or infected with *Toxoplasma* (obtained from syringe-lysing infected HFFs and trituration). MEFs on coverslips were fixed in prewarmed cDMEM containing 3.7% formaldehyde for 15 min and imaged using a Leica DFC425 camera with an automated Leica DM5000B microscope and LAS. For imaging of the mitochondrial network and RC_{12} distribution, 2μm z-stacks at 0.1 μm (WT-mitoYFP MEFs) or 4um z-stacks at 0.1um (*Mfn1*$^{+/+}$,*2*$^{+/+}$ and *Mfn1*$^{-/-}$,*2*$^{-/-}$ MEFs). Fluorescence signals were analyzed using IMIC Andromeda system (Fondis Electronic) equipped with ORCA-03G Camera (Hamamatsu), a 60X oil objective (UPLAN 60X, 1.35NA, Olympus), a 561nm laser for excitation and a FF01-446/523/600/677 emission filter (Semrock). The Manders 2 coefficient, or fraction of RC_{12} signal overlapping mitochondrial YFP, was determined from Z-stack projections of RC_{12} and mitochondrial YFP using the Fiji JACoP plugin. For analysis of mitochondrial morphology, mitochondria

segmentation was performed using the ImageJ Squassh (Rizk et al., 2014) plugin, and size and morphology characteristics were performed using Fiji.

Flow Cytometry Analysis of Parasites

MEFs were plated in 12 or 24 well-plates and pulsed with BODIPY FL C_{12} overnight. Following 14-16h of labeling, monolayers were rinsed twice in prewarmed HBSS1X and *RFP*$^{+}$-*Toxoplasma* parasites were added at a multiplicity of infection (MOI) of 10 (of initial number of MEFs plated). Twenty-four hpi, MEFs were trypsinized, briefly centrifuged and resuspended in prewarmed 0.005% digitonin in PBS for 5 minutes. Cells were triturated ten times by passing them through an insulin syringe, spun down and resuspended in 4% paraformaldehyde in FACS buffer for 20min. After a brief spin, cells were resuspended in FACS buffer and analyzed for the FL C_{12} mean fluorescence intensity (MFI) using CellQuest Pro on a FACScalibur (BD Biosciences).

Flow Cytometry Analysis of Infection

For all infections, MEFs were plated in either 12- or 24- wells and the following day, or when monolayers were at a confluency of ~70%, infected with *Toxoplasma* at an MOI of 2. Two hpi, infected monolayers were washed twice with serum-free media to rinse off extracellular parasites and either incubated in cDMEM alone or supplemented with the following inhibitors or reagents from Sigma-Aldrich: syntheChol NS0, linoleic acid-oleic acid-albumin, atglistatin (as indicated), GW0742 (50μM), and etomoxir (200μM), pyrimethamine (40μM), and MitoTEMPO (20μM) At 24hpi, cells were rinsed with PBS, trypsinized and fixed in 2% paraformaldehyde in FACS buffer (3% FBS in PBS) for 10min. After a brief spin, cells were resuspended in FACS buffer and sorted on a FACScalibur (BD Biosciences) and analyzed for median FI (mFI) using CellQuest Pro, at least s000 infected cells counted per sample. Infected cells were identified by the red fluorescence of the transgenic *Toxoplasma*. If provided, brightfield and fluorescence images of live monolayers were captured at 24hpi with a DFC300FX Digital Color Camera on an inverted Leica DMI4000B scope and processed using the Leica Application Suite (LAS).

Plaque Assay

MEFs were plated in T25 flasks and infected with 100 parasites of the Type I (RH*Δhxgprt*) strain. 7 dpi, flasks were rinsed with methanol, incubated in crystal violet for 20 minutes, and rinsed. Plaques were using an inverted Leica DMI4000B scope and processed using the Leica Application Suite (LAS).

QUANTIFICATION AND STATISTICAL ANALYSIS

Data are presented as mean±SEM unless otherwise indicated in figure legends. Sample numbers and experimental repeats are indicated in the figures legends. All data were analyzed using the unpaired student's t-test, one-way ANOVA, or two-way ANOVA, as indicated in the figure legends. For all experiments p values < 0.05 were considered significant.